BULLETIN OF THE EARTHQUAKE
RESEARCH INSTITUTE
Vol. 47 (1969), pp. 1-29

1. *Stress Fields in the Neighborhood of a Crack.*

By Takuo MARUYAMA,

Earthquake Research Institute.

(Read October 22 and November 26, 1968.—Received November 30, 1968.)

Abstract

Two-dimensional crack models in a purely elastic homogeneous medium with various boundary conditions on the crack surface are studied from the view-point of superposed two-dimensional Somigliana dislocations on a uniform stress field. Formulas obtained in the previous study are employed and 24 or more contour maps are given which show the stress distribution around a crack.

Contents

1. Introduction

Displacements, strains and stresses associated with a fault are of geophysical interest. However, as for a fault model which permits of

mathematical treatments we must concern ourselves with fairly idealized situations for the present. The representation of a fault as a dislocation surface (Vvedenskaya, 1956; Steketee, 1958a, b) has much merit and has been developed in many papers (e.g. Chinnery, 1961, 1963; Maruyama, 1963, 1964; Press, 1965). Here, we use the term 'dislocation' in the sense of Somigliana dislocation (e.g. Eshelby, 1956) or in the sense of displacement discontinuity which causes a Somigliana dislocation.

Particularly the stress distribution around faults is of tectonophysical interest. If we assume a dislocation surface in a semi-infinite elastic medium, it is possible to calculate components of stress throughout the medium surrounding the fault, for a variety of model shapes and orientations (Maruyama, 1964). For the case of strike slip fault of rectangular plane, stress distributions on the ground surface are shown in the form of contour or trajectory maps (Chinnery, 1963, 1966; Chinnery and Petrak, 1968). However, two-dimensional formulation of the problem is of more fundamental nature and has a great advantage of simplicity. In fact, the two-dimensional model of a crack received much attention since the days of Inglis (1913). A model of this kind by Starr (1928) has recently been applied to the estimation of stress drop at the earthquake sources (e.g Aki, 1966). To our knowledge, however, contour or trajectory maps which make clear the stress distribution around a two-dimensional crack fail to be available except those by Sneddon (1946; 1951, p. 429) and Anderson (1951, p. 163), although maps of the stress distribution around holes in the book of Savin (1961) should be mentioned.

It is our main purpose in this paper to add contour maps to those which are now available for us. The stress field is expressed by two-dimensional Somigliana dislocations or by superpositions of such dislocations on a uniform stress field. Not only the cracks of slip type as employed as a model of a fault but also the crack models, in which the surfaces of the crack have moved in the direction of normal, are included in the present paper. It seems that these models have some merit in rock mechanics or in model experiments.

In the present study we confine ourselves to the linear theory of elasticity and non-linear formulations as "problems with unknown boundaries" (Barenblatt, 1962) are not discussed. We restrict ourselves to the stress fields around cracks of 'System II' defined in our previous paper (Maruyama, 1966), and two-dimensional cracks as studied by Kasahara (1957) and Knopoff (1958) are not included. They belong to 'System I' in our previous paper and the corresponding stress fields have much simpler features than the present cases.

By assuming an elliptic type two-dimensional discontinuity in displacement, perpendicular to the crack, Steketee (1958b) constructed a solution

which is not different from the stress field due to a crack opened by a uniform pressure (Sneddon 1951, p. 428). Under the words 'elliptic type discontinuity' we mean that the discontinuity is proportional to $(a^2-\xi^2)^{1/2}$, where the width of the crack is $2a$ and ξ is the distance from the midpoint of the crack. In like manner, by assuming an elliptic type discontinuity in displacement, parallel to the crack, we are to obtain a field due to a crack with slipped surfaces in a uniform shear stress. The identity of this field with Starr's (1928) is shown in Appendix (§ 7.1).

2. Preliminary analysis

In the first place we prepare the two-dimensional transformation formulas of stress components for the sake of later reference. Let the components of stress referred to the axes x, y be denoted by τ_{xx}, τ_{yy}, τ_{xy}, and those referred to ξ, η by $\tau_{\xi\xi}$, $\tau_{\eta\eta}$, $\tau_{\xi\eta}$. Two coordinates are related by the following orthogonal scheme of transformation, ϕ being the angle between the x-axis and the ξ-axis, measured counterclokwise from the direction of the x-axis (Fig. 1).

	x	y
ξ	$\cos\phi$	$\sin\phi$
η	$-\sin\phi$	$\cos\phi$

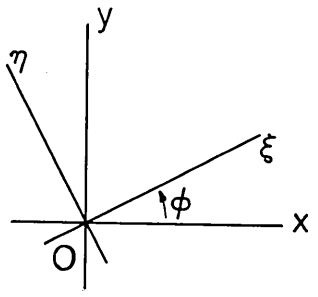

Fig. 1. Two rectangular coordinate systems.

Then we have

$$\begin{cases} \tau_{\xi\xi}=\dfrac{\tau_{xx}+\tau_{yy}}{2}+\dfrac{\tau_{xx}-\tau_{yy}}{2}\cos 2\phi+\tau_{xy}\sin 2\phi \\ \tau_{\eta\eta}=\dfrac{\tau_{xx}+\tau_{yy}}{2}-\dfrac{\tau_{xx}-\tau_{yy}}{2}\cos 2\phi-\tau_{xy}\sin 2\phi \\ \tau_{\xi\eta}=-\dfrac{\tau_{xx}-\tau_{yy}}{2}\sin 2\phi+\tau_{xy}\cos 2\phi. \end{cases} \tag{2.1}$$

If $O\xi$ and $O\eta$ are the principal axes (the third principal axis being perpendicular to the $\xi\eta$-plane), $\tau_{\xi\eta}=0$. Denoting $\tau_{\xi\xi}$ and $\tau_{\eta\eta}$ by N_1 and N_2 respectively, we have the following relations,

$$\begin{cases} \dfrac{\tau_{xx}+\tau_{yy}}{2}=\dfrac{N_1+N_2}{2} \\ \dfrac{\tau_{xx}-\tau_{yy}}{2}=\dfrac{N_1-N_2}{2}\cos 2\phi \\ \tau_{xy}=\dfrac{N_1-N_2}{2}\sin 2\phi. \end{cases} \tag{2.2}$$

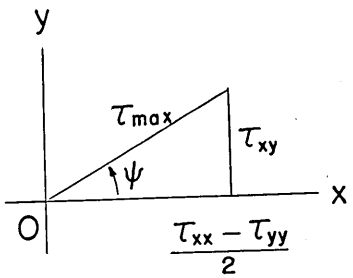

Fig. 2. Construction of ϕ from which direction of maximum tesion is found.

From these equations if τ_{xx}, τ_{yy}, and τ_{xy} are known at a point, and if we assume that $N_1>N_2$, ϕ can be obtained by constructing a vector of which x-, y- components are $(\tau_{xx}-\tau_{yy})/2$ and τ_{xy} respectively (Fig. 2). Denoting the angle between the radius and the x-axis measured counterclockwise from the x-axis by ϕ, the value of N_1 and its direction are found to be

$$\begin{cases} N_1=\dfrac{\tau_{xx}+\tau_{yy}}{2}+\sqrt{\left(\dfrac{\tau_{xx}-\tau_{yy}}{2}\right)^2+\tau_{xy}^2} \\ \phi=\dfrac{\psi}{2}, \qquad \dfrac{\psi}{2}\pm\pi. \end{cases} \tag{2.3}$$

Since we take tension as positive, these formulas give the maximum tension $\sigma_{\max}$ and its direction. The maximum shear stress $\tau_{\max}$ is obtained from the third equation of (2.1) as

$$\tau_{\max}=\sqrt{\left(\frac{\tau_{xx}-\tau_{yy}}{2}\right)^2+\tau_{xy}^2}. \tag{2.4}$$

Next, we consider the elastic field caused by a given discontinuity in displacement along a segment L. Let this segment be $(-a, a)$ on the x-axis and the discontinuity in displacement be

$$\begin{cases} u^+(\xi)-u^-(\xi)=\Delta u(\xi) \\ v^+(\xi)-v^-(\xi)=\Delta v(\xi) \end{cases} \quad \text{on} \quad L\ (-a\leqq\xi\leqq a), \tag{2.5}$$

where u and v denote the x- and y- component of displacement and the superscripts + and − correspond to the values on the positive and negative sides of the segment respectively. We take the positive side of the segment in accord with the positive direction of the y-axis (Fig. 3). Equations (2.5) are combined as

$$\Delta u(\xi)+i\Delta v(\xi)=g(\xi). \tag{2.6}$$

The field at any point (x, y) can be expressed by the use of functions of

$$z=x+iy, \qquad \bar{z}=x-iy. \tag{2.7}$$

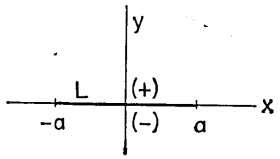

Fig. 3. Positive and negative sides of L.

An elastic constant κ is introduced which is expressed by means of the Lamé's constants (λ, μ) or Poisson's ratio σ as

$$\kappa=\frac{\lambda+3\mu}{\lambda+\mu}=3-4\sigma \tag{2.8}$$

in the case of plane strain, while as

$$\kappa=\frac{5\lambda+6\mu}{3\lambda+2\mu}=\frac{3-\sigma}{1+\sigma} \tag{2.9}$$

in the case of generalized plane stress (thin plates) (e.g. Muskhelishvili, 1953, p. 112). The field due to the dislocation (2.5) can then be obtained as in equations (5.11), (5.13) and (5.15) in the previous paper (Maruyama, 1966):

$$\begin{cases} 2\mu(u+iv)=\kappa\varphi(z)-\varphi(\bar{z})-(z-\bar{z})\overline{\varphi'(z)} \\ \dfrac{\tau_{xx}+\tau_{yy}}{2}=\varphi'(z)+\overline{\varphi'(z)} \\ \dfrac{\tau_{xx}-\tau_{yy}}{2}+i\tau_{xy}=-\varphi'(\bar{z})+\overline{\varphi'(z)}-(z-\bar{z})\overline{\varphi''(z)} \end{cases} \tag{2.10}$$

where

$$\varphi(z)=\frac{2\mu}{\kappa+1}\frac{1}{2\pi i}\int_{-a}^{a}\frac{g(\xi)}{\xi-z}d\xi. \tag{2.11}$$

When the discontinuity in displacement is either perpendicular or parallel to L, simple relations hold, and we have

$$\varphi(\bar{z})=-\overline{\varphi(z)}, \quad \text{if} \quad \Delta v=0, \tag{2.12}$$

and

$$\varphi(\bar{z})=\overline{\varphi(z)}, \quad \text{if} \quad \Delta u=0, \tag{2.13}$$

which correspond to the case of a shear crack and to that of a tension crack respectively.

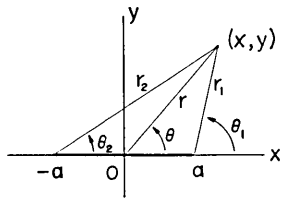

Fig. 4. Polar coordinates r, θ and coordinates r_1, r_2, θ_1, θ_2.

It is convenient to introduce coordinates r_1, r_2, θ_1, θ_2 (Fig. 4) defined by

$$z-a=r_1e^{i\theta_1}, \qquad z+a=r_2e^{i\theta_2}, \tag{2.14}$$

as well as polar coordinates r, θ defined by

$$z=re^{i\theta}, \tag{2.15}$$

to obtain the expressions separated in real and imaginary parts.

3. A simple model of the crack end

By use of the foregoing expressions we can calculate the stress distribution around any dislocation. When the displacement discontinuity has a very sharp variation in the vicinity of the end of L, a singularity of the stress arises. In such cases the absolute values of stress components become very large in the vicinity of the end of L, and therefore even if the dislocation is placed in a previously strained state, we can see the main feature of the stress distribution by neglecting the initial stresses.

When the displacement discontinuity is constant (not zero) on L and zero on all the other parts of x-axis, we have extremely simple stress fields. This discontinuity may be called rectangular type. If we put

$$\Delta u=U=\text{const.} \quad \text{on} \quad L \tag{3.1}$$

or

$$\Delta v=V=\text{const.} \quad \text{on} \quad L, \tag{3.2}$$

then we have, for the tangential discontinuity,

$$\varphi(z)=\frac{2\mu}{\kappa+1}\frac{U}{2\pi i}\left\{\log(z-a)-\log(z+a)\right\} \tag{3.3}$$

from which we can obtain

$$\left\{\begin{aligned}
\frac{\tau_{xx}+\tau_{yy}}{2}&=\frac{2\mu}{\kappa+1}\frac{U}{\pi}\left(-\frac{1}{r_1}\sin\theta_1+\frac{1}{r_2}\sin\theta_2\right)\\
\frac{\tau_{xx}-\tau_{yy}}{2}&=\frac{2\mu}{\kappa+1}\frac{U}{\pi}\left\{-\frac{1}{r_1}\sin\theta_1+\frac{1}{r_2}\sin\theta_2\right.\\
&\qquad\left.+y\left(-\frac{1}{r_1^2}\cos 2\theta_1+\frac{1}{r_2^2}\cos 2\theta_2\right)\right\}\\
\tau_{xy}&=\frac{2\mu}{\kappa+1}\frac{U}{\pi}\left\{\frac{1}{r_1}\cos\theta_1-\frac{1}{r_2}\cos\theta_2\right.\\
&\qquad\left.+y\left(-\frac{1}{r_1^2}\sin 2\theta_1+\frac{1}{r_2^2}\sin 2\theta_2\right)\right\}.
\end{aligned}\right. \tag{3.4}$$

For the normal discontinuity,

$$\varphi(z)=\frac{2\mu}{\kappa+1}\frac{V}{2\pi}\{\log(z-a)-\log(z+a)\} \tag{3.5}$$

from which we can obtain

$$\begin{cases} \dfrac{\tau_{xx}+\tau_{yy}}{2}=\dfrac{2\mu}{\kappa+1}\dfrac{V}{\pi}\left(\dfrac{1}{r_1}\cos\theta_1-\dfrac{1}{r_2}\operatorname{con}\theta_2\right) \\ \dfrac{\tau_{xx}-\tau_{yy}}{2}=\dfrac{2\mu}{\kappa+1}\dfrac{V}{\pi}y\left(-\dfrac{1}{r_1^2}\sin 2\theta_1+\dfrac{1}{r_2^2}\sin 2\theta_2\right) \\ \tau_{xy}=\dfrac{2\mu}{\kappa+1}\dfrac{V}{\pi}y\left(\dfrac{1}{r_1^2}\cos 2\theta_1-\dfrac{1}{r_2^2}\cos 2\theta_2\right). \end{cases} \tag{3.6}$$

If we put $r_2=\infty$, we obtain the stresses in the neighborhood of the right end of the crack. Defining D and χ (Fig. 5) by

$$U=D\cos\chi, \qquad V=D\sin\chi, \tag{3.7}$$

we have the stress fields corresponding to superposition of the tangential and normal discontinuities as follows:

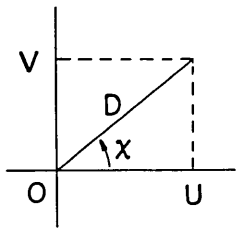

Fig. 5. Definition of D and χ.

$$\begin{cases} \dfrac{\tau_{xx}+\tau_{yy}}{2}=\dfrac{2\mu}{\kappa+1}\dfrac{D}{\pi}\dfrac{1}{r_1}\{-\sin(\theta_1-\chi)\} \\ \dfrac{\tau_{xx}-\tau_{yy}}{2}=\dfrac{2\mu}{\kappa+1}\dfrac{D}{\pi}\dfrac{1}{r_1}\{-\cos(\theta_1-\chi)\}\sin 2\theta_1 \\ \tau_{xy}=\dfrac{2\mu}{\kappa+1}\dfrac{D}{\pi}\dfrac{1}{r_1}\{\cos(\theta_1-\chi)\}\cos 2\theta_1. \end{cases} \tag{3.8}$$

From these equations we obtain

$$\begin{cases} \tau_{\max}=\dfrac{2\mu}{\kappa+1}\dfrac{D}{\pi}\dfrac{1}{r_1}|\cos(\theta_1-\chi)| \\ \sigma_{\max}=\dfrac{2\mu}{\kappa+1}\dfrac{D}{\pi}\dfrac{1}{r_1}\{|\cos(\theta_1-\chi)|-\sin(\theta_1-\chi)\} \\ \dot{\varphi}=\theta_1-\dfrac{\pi}{4}. \end{cases} \tag{3.9}$$

When $\chi=0$, the distributions of maximum shear stress and maximum tension are shown in Fig. 6. We can see from equations (3.9) that the corresponding field around the right end for any χ can be obtained by rotating the field of the case $\chi=0$ counterclockwise by the angle χ.

Schematic representation of the form of displacements of the crack surfaces and the corresponding distributions of maximum shear stress at the right end are shown in Fig. 7.

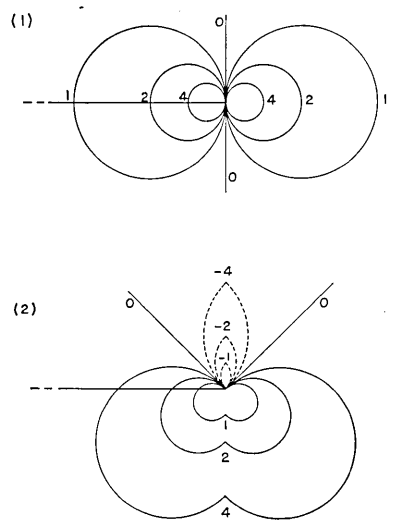

Fig. 6. (1): Contours of equal maximum shear stress around the right end of the crack; (2): Contours of equal maximum tension, around the right end of the crack. Contour values are in arbitrary scale.

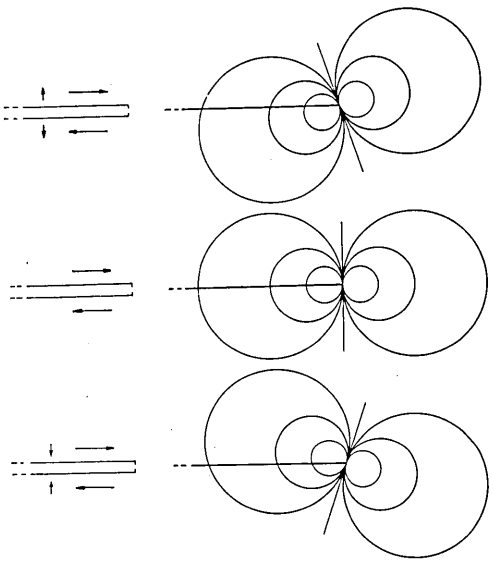

Fig. 7. Rotation of the maximum shear stress field around the right end, corresponding to the ratio of normal and tangential discontinuities in displacement.

4. Models in which the crack surfaces are assumed to be free, under a uniform stress

If we take the elliptic type of displacement discontinuity on the segment as

$$\Delta u = U\sqrt{1-\left(\frac{\xi}{a}\right)^2} \qquad \text{on } L \tag{4.1}$$

or

$$\Delta v = V\sqrt{1-\left(\frac{\xi}{a}\right)^2} \qquad \text{on } L, \tag{4.2}$$

where U and V are the values of discontinuty at the center of L, we have the constant values of τ_{xy} and τ_{yy} on the segment due to this dislocation.

In the case of parallel discontinuity (4.1) we have (c.f. Maruyama, 1966)

$$\varphi(z)=\frac{2\mu}{\kappa+1}\frac{U}{2a}(\sqrt{a^2-z^2}+iz), \tag{4.3}$$

while in the case of perpendicular discontinuity (4.2) we have

$$\varphi(z)=\frac{2\mu}{\kappa+1}\frac{V}{2a}(i\sqrt{a^2-z^2}-z). \tag{4.4}$$

As to the function $\sqrt{a^2-z^2}$ in equations (4.3) and (4.4), the branch for which it takes the positive value on the positive side of the segment L is selected (Maruyama, 1966). Using coordinates r_1, r_2, θ_1, θ_2, the adopted branch is written by equation (2.14) as

$$\sqrt{a^2-z^2}=\sqrt{r_1r_2}e^{i\left(\frac{\theta_1+\theta_2}{2}-\frac{\pi}{2}\right)}. \tag{4.5}$$

By use of these coordinates and polar coordinates, we obtain the components of displacement and stress for the discontinuity (4.1) as follows:

$$\left\{\begin{aligned}
2\mu u&=\frac{2\mu}{\kappa+1}\frac{U}{a}\left[\frac{\kappa+1}{2}\left(\sqrt{r_1r_2}\sin\frac{\theta_1+\theta_2}{2}-r\sin\theta\right)\right.\\
&\qquad\left.+r\sin\theta\left\{-1+\frac{r}{\sqrt{r_1r_2}}\cos\left(\theta-\frac{\theta_1+\theta_2}{2}\right)\right\}\right]\\
2\mu v&=\frac{2\mu}{\kappa+1}\frac{U}{a}\left[-\frac{\kappa-1}{2}\left(\sqrt{r_1r_2}\cos\frac{\theta_1+\theta_2}{2}-r\cos\theta\right)\right.\\
&\qquad\left.+r\sin\theta\left\{-\frac{r}{\sqrt{r_1r_2}}\sin\left(\theta-\frac{\theta_1+\theta_2}{2}\right)\right\}\right]
\end{aligned}\right. \tag{4.6}$$

$$\left\{\begin{aligned}
\frac{\tau_{xx}+\tau_{yy}}{2}&=\frac{2\mu}{\kappa+1}\frac{U}{a}\frac{r}{\sqrt{r_1r_2}}\sin\left(\theta-\frac{\theta_1+\theta_2}{2}\right)\\
\frac{\tau_{xx}-\tau_{yy}}{2}&=\frac{2\mu}{\kappa+1}\frac{U}{a}\left\{\frac{r}{\sqrt{r_1r_2}}\sin\left(\theta-\frac{\theta_1+\theta_2}{2}\right)\right.\\
&\qquad\left.-\frac{a^2r}{(r_1r_2)^{3/2}}\sin\theta\cos\frac{3(\theta_1+\theta_2)}{2}\right\}\\
\tau_{xy}&=\frac{2\mu}{\kappa+1}\frac{U}{a}\left\{-1+\frac{r}{\sqrt{r_1r_2}}\cos\left(\theta-\frac{\theta_1+\theta_2}{2}\right)\right.\\
&\qquad\left.-\frac{a^2r}{(r_1r_2)^{3/2}}\sin\theta\sin\frac{3(\theta_1+\theta_2)}{2}\right\}.
\end{aligned}\right. \tag{4.7}$$

Comparison of the displacements (4.6) with Starr's (1928) is made in Appendix (§ 7.1).

The corresponding expressions for the discontinuity (4.2) are as follows:

$$\left\{\begin{aligned} 2\mu u &= \frac{2\mu}{\kappa+1}\frac{V}{a}\left[\frac{\kappa-1}{2}\left(\sqrt{r_1r_2}\cos\frac{\theta_1+\theta_2}{2}-r\cos\theta\right)\right.\\ &\qquad\left.-\frac{r^2}{\sqrt{r_1r_2}}\sin\theta\sin\left(\theta-\frac{\theta_1+\theta_2}{2}\right)\right]\\ 2\mu v &= \frac{2\mu}{\kappa+1}\frac{V}{a}\left[\frac{\kappa+1}{2}\left(\sqrt{r_1r_2}\sin\frac{\theta_1+\theta_2}{2}-r\sin\theta\right)\right.\\ &\qquad\left.-r\sin\theta\left\{-1+\frac{r}{\sqrt{r_1r_2}}\cos\left(\theta-\frac{\theta_1+\theta_2}{2}\right)\right\}\right] \end{aligned}\right. \tag{4.8}$$

$$\left\{\begin{aligned} \frac{\tau_{xx}+\tau_{yy}}{2} &= \frac{2\mu}{\kappa+1}\frac{V}{a}\left\{-1+\frac{r}{\sqrt{r_1r_2}}\cos\left(\theta-\frac{\theta_1+\theta_2}{2}\right)\right\}\\ \frac{\tau_{xx}-\tau_{yy}}{2} &= \frac{2\mu}{\kappa+1}\frac{V}{a}\left\{-\frac{a^2r}{(r_1r_2)^{3/2}}\sin\theta\sin\frac{3(\theta_1+\theta_2)}{2}\right\}\\ \tau_{xy} &= \frac{2\mu}{\kappa+1}\frac{V}{a}\left\{\frac{a^2r}{(r_1r_2)^{3/2}}\sin\theta\cos\frac{3(\theta_1+\theta_2)}{2}\right\}. \end{aligned}\right. \tag{4.9}$$

Equations (4.9) are the same as the expressions of stress due to a crack opened by a uniform pressure (Sneddon, 1951, p. 428; Green and Zerna, 1954, p. 279; Steketee, 1958b).

The forces acting on the segment L per unit length for these cases are obtained from equations (4.7) and (4.9). We have for the discontinuity (4.1)

$$\tau_{xy}=-\frac{2\mu}{\kappa+1}\frac{U}{a}, \qquad \tau_{yy}=0 \quad \text{on} \quad L, \tag{4.10}$$

and for the discontinuity (4.2)

$$\tau_{xy}=0, \qquad \tau_{yy}=-\frac{2\mu}{\kappa+1}\frac{V}{a} \quad \text{on} \quad L. \tag{4.11}$$

At this point we can construct the stress field including a crack under a uniform stress. The uniform stress field is expressed by the equation (2.2) with N_1, N_2 and $\dot{\varphi}$ as constants. The field in which the crack surfaces are assumed to be free can be obtained by the superposition of three stress fields

$$(2.2)+(4.7)+(4.9) \tag{4.12}$$

under the condition

$$\begin{cases} \tau_{xy}=\dfrac{N_1-N_2}{2}\sin 2\phi-\dfrac{2\mu}{\kappa+1}\dfrac{U}{a}=0 \\ \tau_{yy}=\dfrac{N_1+N_2}{2}-\dfrac{N_1-N_2}{2}\cos 2\phi-\dfrac{2\mu}{\kappa+1}\dfrac{V}{a}=0 \end{cases} \tag{4.13}$$

It can be proved after some calculation that the solution constructed is identical to the solution in the book of Muskhelishvili (1953, p. 508).

4.1 Models under a uniform pure shear stress

The stress fields with a crack under a uniform pure shear stress are shown in Figs. 8 and 9, separately for τ_{xx}, τ_{yy}, τ_{xy}, maximum shear stress, maximum tension and direction of maximum tension. We take the values of N_1 and N_2 in (4.13) as

$$N_1=100, \qquad N_2=-100 \tag{4.14}$$

in every Figure and

$$\phi=45^\circ \quad \left(\text{hence } U=100\left(\frac{\kappa+1}{2\mu}\right)a, \qquad V=0\right) \tag{4.15}$$

in Figs. 8; a), b), $\cdots$, f); while

$$\phi=60^\circ \quad \left(\text{hence } U=50\sqrt{3}\left(\frac{\kappa+1}{2\mu}\right)a, \qquad V=50\left(\frac{\kappa+1}{2\mu}\right)a\right) \tag{4.16}$$

in Figs. 9; g), h), $\cdots$, l).

It is seen from the equations (4.13), (4.14) and (4.15) that in the case of Fig. 8, when $V=0$, the stress field (4.9) has no relation to the resultant field. One of the differences, which appear in the maps of maximum shear stress, between the stress fields, expressed in equations (4.7) and (4.9), can be found from the comparison of Fig. 8, d) with Fig. 85 in the book of Sneddon (1951, p. 429): we have at the ends of a crack contours of shape of a section of a gourd in the former case, while those of shape of the letter '8' in the latter. Directions of principal stresses may be shown more clearly than in Fig. 8, f) by means of 'isostatic lines' (Anderson, 1951) which everywhere contain the direction of principal stress. Comparison of Fig. 8, f) with Fig. 35 in the book of Anderson (1951, p. 163) makes clear the correspondence of two methods.

4.2 Models under a uniform uniaxial pressure

The fields with a crack which is open under a uniform uniaxial pressure are shown in Fig. 10 and Fig. 11, separately for maximum

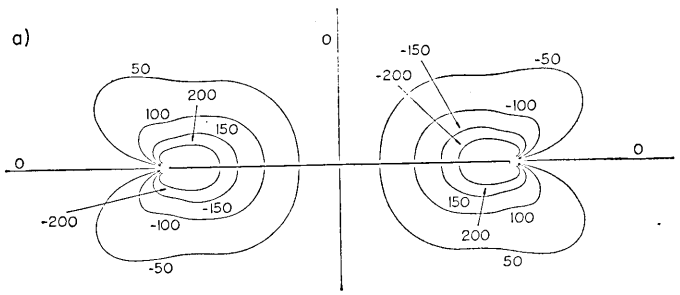

Fig. 8. a) Contours of equal τ_{xx}.

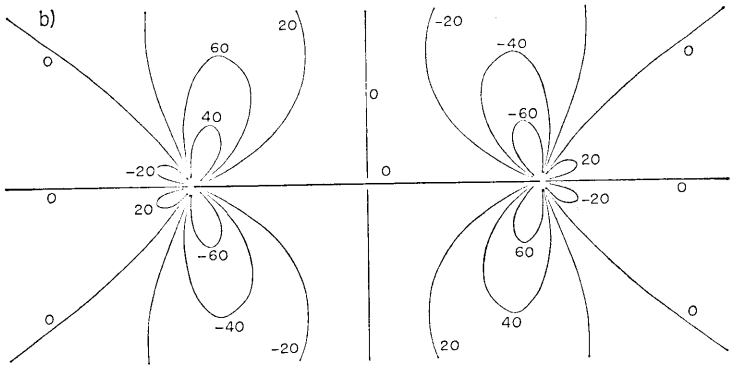

Fig. 8. b) Contours of equal τ_{yy}.

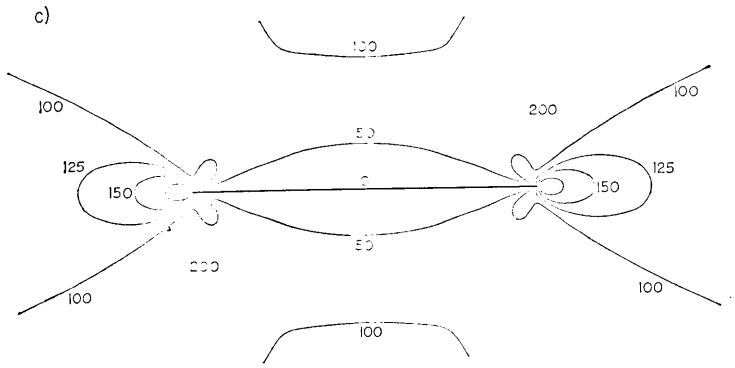

Fig. 8. c) Contours of equal τ_{xy}.

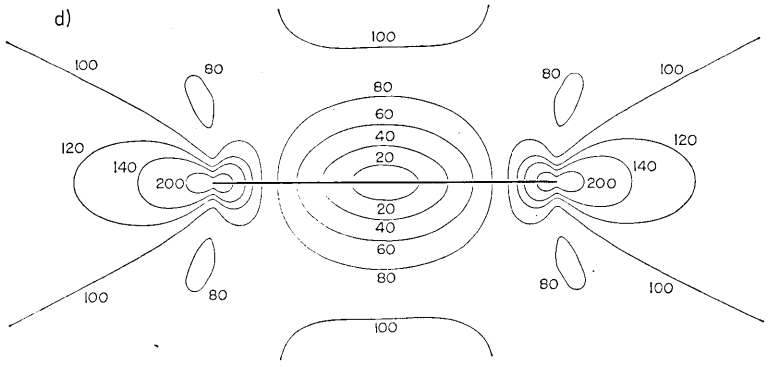

Fig. 8. d) Contours of equal maximum shear stress.

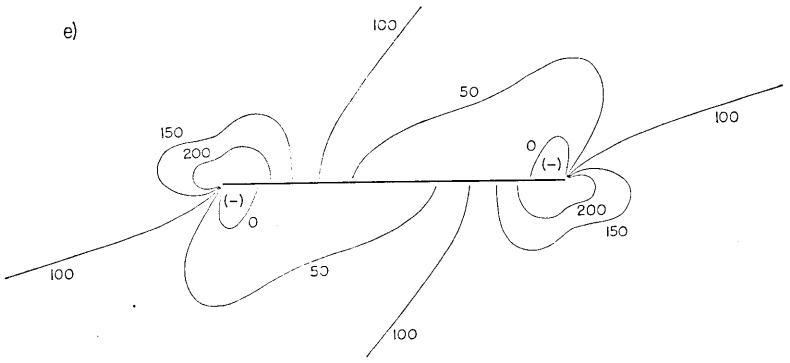

Fig. 8. e) Contours of equal maximum tension.

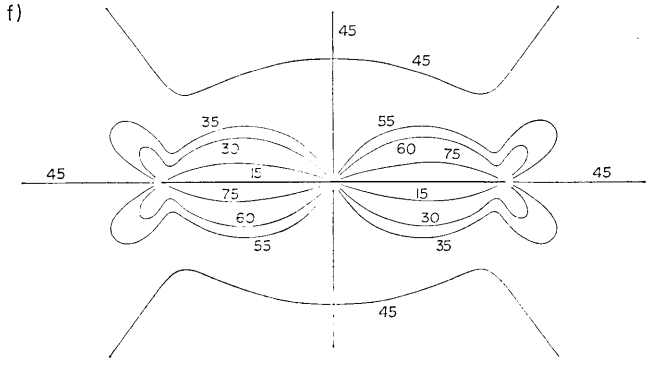

Fig. 8. f) Contours of equal direction of maximum tension. Contour values are in units of degrees, measured counterclockwise from the direction of x-axis.

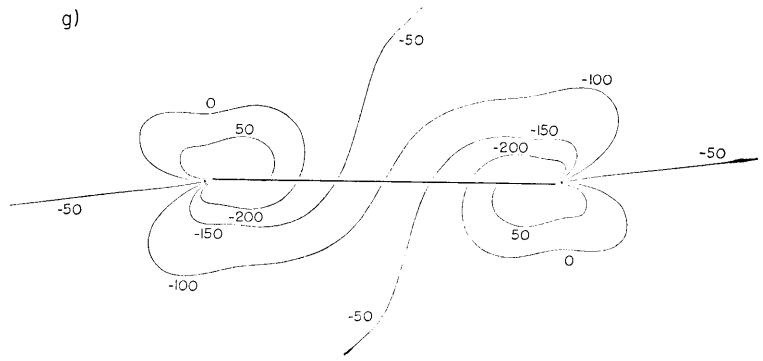

Fig. 9. g) Contours of equal τ_{xx}.

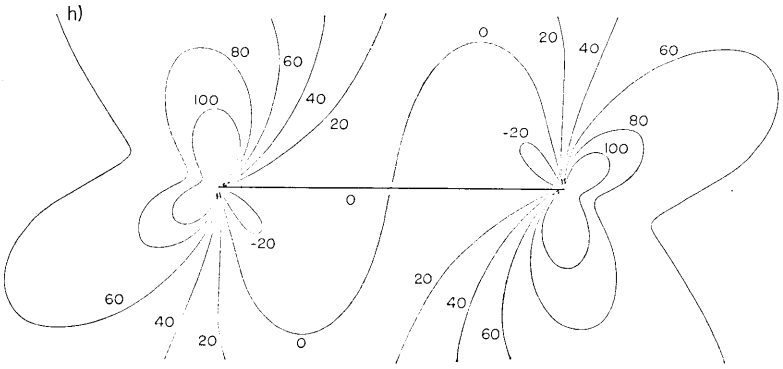

Fig. 9. h) Contours of equal τ_{yy}.

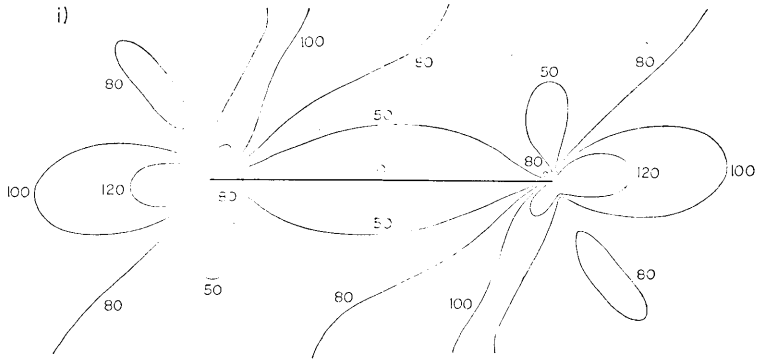

Fig. 9. i) Contours of equal τ_{xy}.

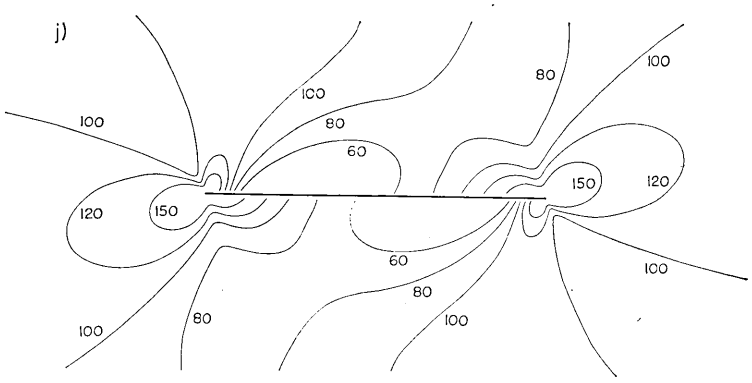

Fig. 9. j) Contours of equal maximum shear stress.

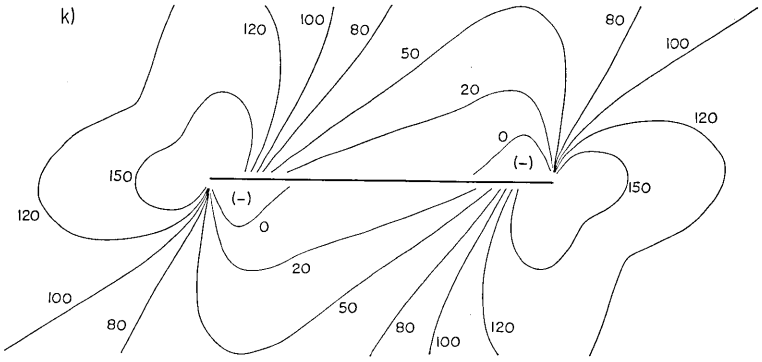

Fig. 9. k) Contours of equal maximum tension.

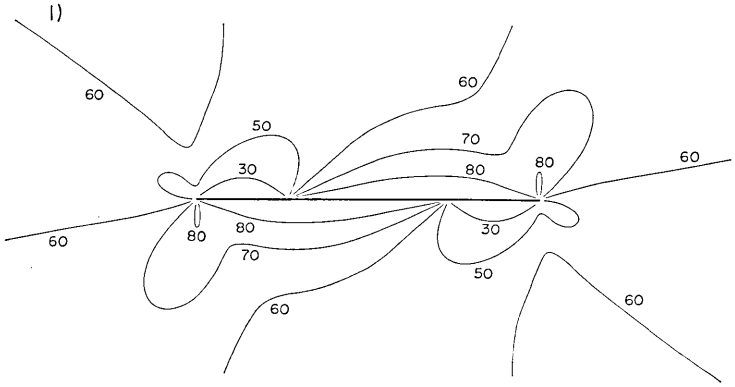

Fig. 9. l) Contours of equal direction of maximum tension. Contour values are in units of degrees, measured counterclockwise from the direction of x-axis.

shear stress, maximum tension and direction of maximum tension. We take the values of N_1 and N_2 in (4.13) as

$$N_1=0, \qquad N_2=-200 \tag{4.17}$$

in every Figure and

$$\phi=45^\circ \quad \left(\text{ hence } \quad U=100\left(\frac{\kappa+1}{2\mu}\right)a, \qquad V=-100\left(\frac{\kappa+1}{2\mu}\right)a \right) \tag{4.18}$$

in Fig. 10; m), n) and o); while

$$\phi=60^\circ \quad \left(\text{ hence } \quad U=50\sqrt{3}\left(\frac{\kappa+1}{2\mu}\right)a, \qquad V=-50\left(\frac{\kappa+1}{2\mu}\right)a \right) \tag{4.19}$$

in Fig. 11; p), q) and r).

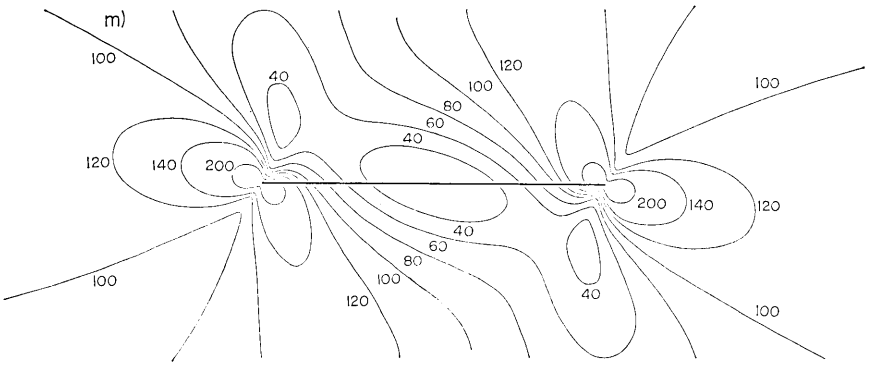

Fig. 10. m) Contours of equal maximum shear stress.

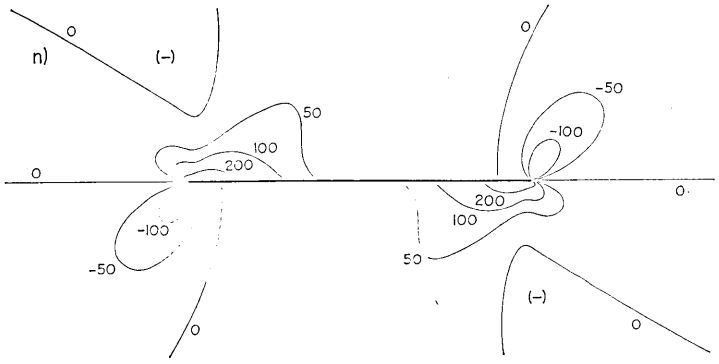

Fig. 10. n) Contours of equal maximum tension.

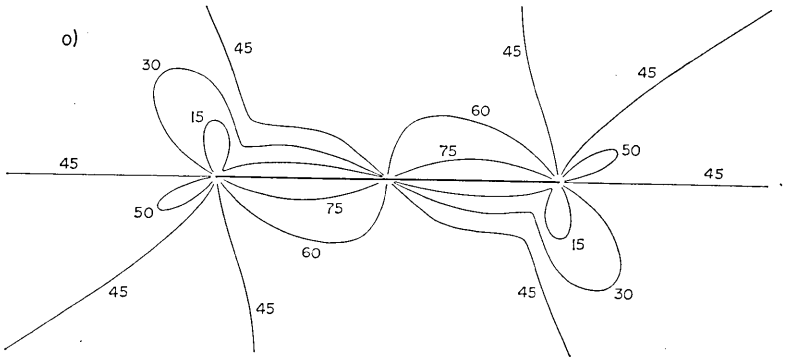

Fig. 10. o) Contours of equal direction of maximum tension. Contour values are in units of degrees, measured counterclockwise from the direction of x-axis.

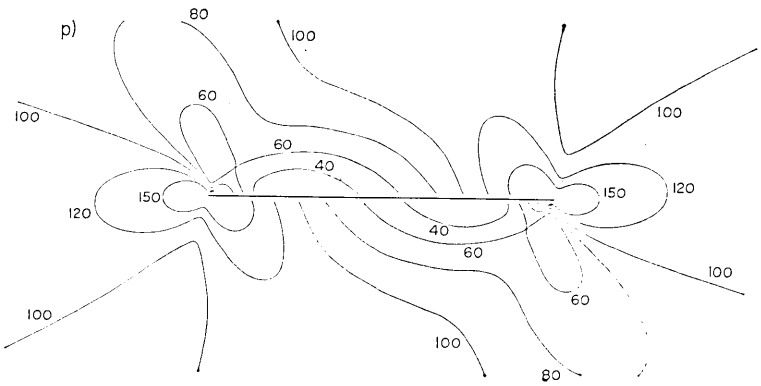

Fig. 11. p) Contours of equal maximum shear stress.

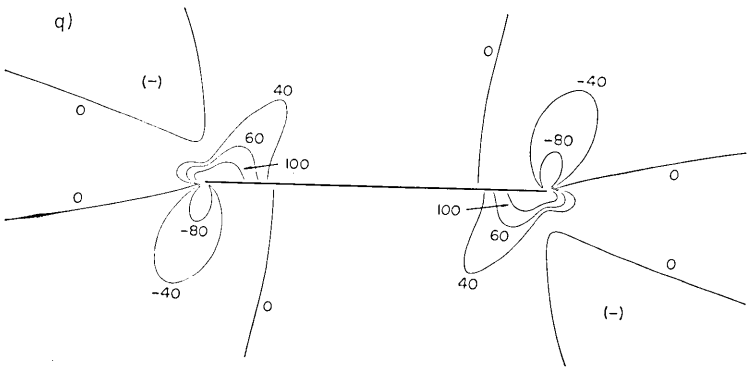

Fig. 11. q) Contours of equal maximum tension.

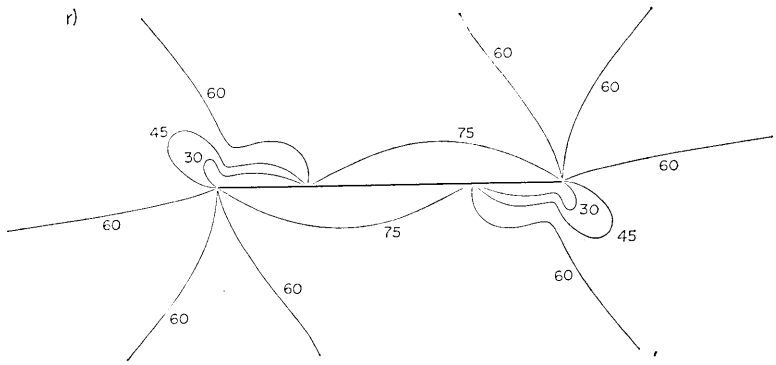

Fig. 11. r) Contours of equal direction of maximum tension. Contour values are in units of degrees, measured counterclockwise from the direction of x-axis.

5. Models in which only the tangential stress on the crack surface is assumed to be decreased, under a uniform stress

The uniform field is expressed by the equations (2.2) with N_1, N_2 and ϕ as constants as before. In this section only the maps of maximum shear stress and of direction of maximum tension are shown, since it is assumed that no movement has occurred in the direction normal to the crack surface and that tension plays no principal part.

5.1 Models in which tangential stress is assumed to vanish on the crack surface throughout

The stress field in which only the tangential stress is assumed to vanish on the crack surface can be obtained by the superposition of two stress fields as

$$(2.2)+(4.7) \tag{5.1}$$

under the condition

$$\begin{cases} \tau_{xy}=\dfrac{N_1-N_2}{2}\sin 2\phi-\dfrac{2\mu}{\kappa+1}\dfrac{U}{a}=0 \\ V=0 \end{cases} \tag{5.2}$$

We take the value in equation (5.2) as

$$\frac{N_1-N_2}{2}=100 \tag{5.3}$$

in every Figure. When

$$\phi=45^\circ \quad \left(\text{hence} \quad U=100\left(\frac{\kappa+1}{2\mu}\right)a, \qquad V=0 \right), \tag{5.4}$$

maps of maximum shear shear stress and of direction of maximum tension are the same as d) and f) in Fig. 1 respectively. In the case when

$$\phi=60^\circ \quad \left(\text{hence} \quad U=50\sqrt{3}\left(\frac{\kappa+1}{2\mu}\right)a, \qquad V=0 \right), \tag{5.5}$$

maximum shear stress and direction of maximum tension are shown in Fig. 12, s) and t).

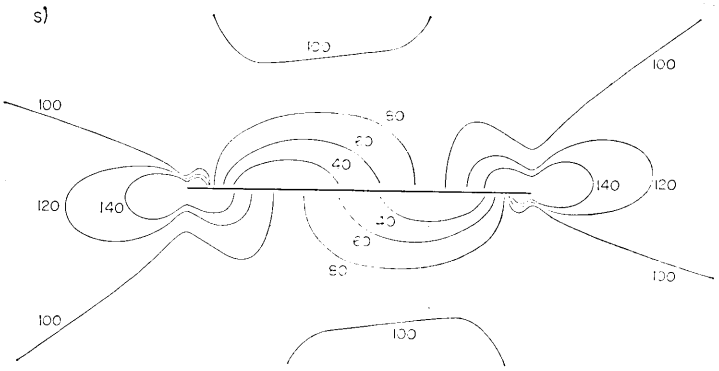

Fig. 12. s) Contours of equal maximum shear stress.

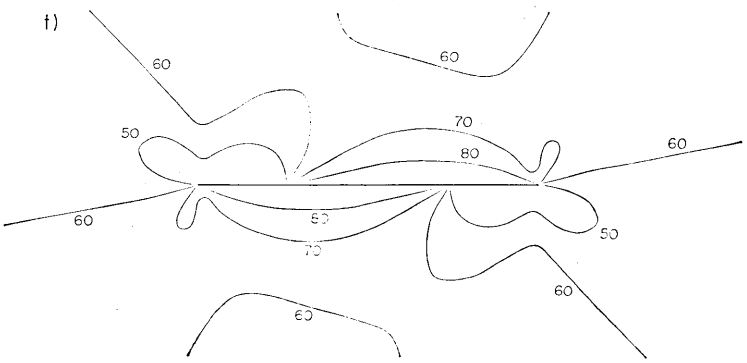

Fig. 12. t) Contours of equal direction of maximum tension. Contour values are in units of degrees, measured counterclockwise from the direction of x-axis.

5.2 *Models in which tangential stress is assumed to vanish at the center and to be decreased at other points on the crack surface*

If we choose the discontinuity in displacement as

$$\Delta u = U\left\{1-\left(\frac{\xi}{a}\right)^2\right\}^{3/2}, \tag{5.6}$$

then we have from equation (2.11) (c.f. Maruyama, 1966)

$$\varphi(z) = \frac{2\mu}{\kappa+1}\frac{U}{2a^3}\left\{(a^2-z^2)^{3/2} - i\left(z^3 - \frac{3}{2}a^2 z\right)\right\} \tag{5.7}$$

from which we can obtain

$$\left\{\begin{aligned}
\frac{\tau_{xx}+\tau_{yy}}{2} &= \frac{2\mu}{\kappa+1}\frac{3U}{a}\left[\left(\frac{r}{a}\right)^2 \sin 2\theta - \frac{r\sqrt{r_1 r_2}}{a^2}\sin\left(\theta+\frac{\theta_1+\theta_2}{2}\right)\right] \\
\frac{\tau_{xx}-\tau_{yy}}{2} &= \frac{2\mu}{\kappa+1}\frac{3U}{a}\left[\left(\frac{r}{a}\right)^2 \sin 2\theta - \frac{r\sqrt{r_1 r_2}}{a^2}\sin\left(\theta+\frac{\theta_1+\theta_2}{2}\right)\right. \\
&\qquad + \frac{r}{a}\sin\theta\left\{2\frac{r}{a}\cos\theta - \frac{\sqrt{r_1 r_2}}{a}\cos\left(\frac{\theta_1+\theta_2}{2}\right)\right. \\
&\qquad \left.\left. - \frac{r^2}{a\sqrt{r_1 r_2}}\cos\left(2\theta - \frac{\theta_1+\theta_2}{2}\right)\right\}\right] \\
\tau_{xy} &= \frac{2\mu}{\kappa+1}\frac{3U}{a}\left[-\frac{1}{2} + \left(\frac{r}{a}\right)^2 \cos 2\theta - \frac{r\sqrt{r_1 r_2}}{a^2}\cos\left(\theta+\frac{\theta_1+\theta_2}{2}\right)\right. \\
&\qquad + \frac{r}{a}\sin\theta\left\{-2\frac{r}{a}\sin\theta + \frac{\sqrt{r_1 r_2}}{a}\sin\left(\frac{\theta_1+\theta_2}{2}\right)\right. \\
&\qquad \left.\left. + \frac{r^2}{a\sqrt{r_1 r_2}}\sin\left(2\theta - \frac{\theta_1+\theta_2}{2}\right)\right\}\right].
\end{aligned}\right. \tag{5.8}$$

The stress components τ_{xy} and τ_{yy} on the x-axis due to this discontinuity in displacement can be written as

$$\left\{\begin{aligned}
\tau_{yy} &= 0, \quad \tau_{xy} = \frac{2\mu}{\kappa+1}\frac{3U}{a}\left\{\left(\frac{\xi}{a}\right)^2 - \frac{1}{2}\right\} && (|\xi| \leqq a) \\
&= \frac{2\mu}{\kappa+1}\frac{3U}{a}\left\{\left(\frac{\xi}{a}\right)^2 - \frac{|\xi|}{a}\sqrt{\left(\frac{\xi}{a}\right)^2 - 1} - \frac{1}{2}\right\} && (|\xi| > a)
\end{aligned}\right. \tag{5.9}$$

In Fig. 13, τ_{xy} on the x-axis is shown. This is a case when the stresses have finite values at the ends of L.

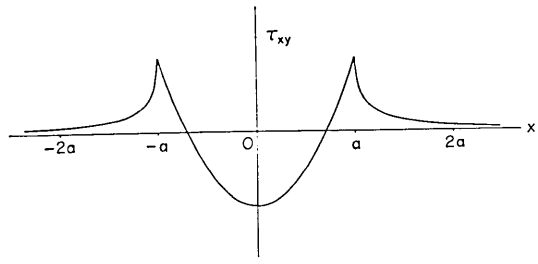

Fig. 13. Shear stress τ_{xy} along the x-axis.

In order to cancel the tangential stress of the uniform stress field at the origin, the following condition must be satisfied:

$$\tau_{xy}=\frac{N_1-N_2}{2}\sin 2\phi-\frac{2\mu}{\kappa+1}\frac{3U}{2a}=0. \tag{5.10}$$

The stress field including the crack can then be expressed by superposition of two stress fields as

$$(2.2)+(5.8). \tag{5.11}$$

We take the value in equation (5.10) as

$$\frac{N_1-N_2}{2}=100 \tag{5.12}$$

in every Figure as before and

$$\phi=45^\circ \quad \left(\text{ hence } \quad U=\frac{200}{3}\left(\frac{\kappa+1}{2\mu}\right)a, \qquad V=0\right) \tag{5.13}$$

in Fig. 14, u) and v); while

$$\phi=65^\circ \quad \left(\text{ hence } \quad U\fallingdotseq 51.07\left(\frac{\kappa+1}{2\mu}\right)a, \qquad V=0\right) \tag{5.14}$$

in Fig. 15, w) and x). It should be noted that ϕ is not equal to 60° in Fig. 15.

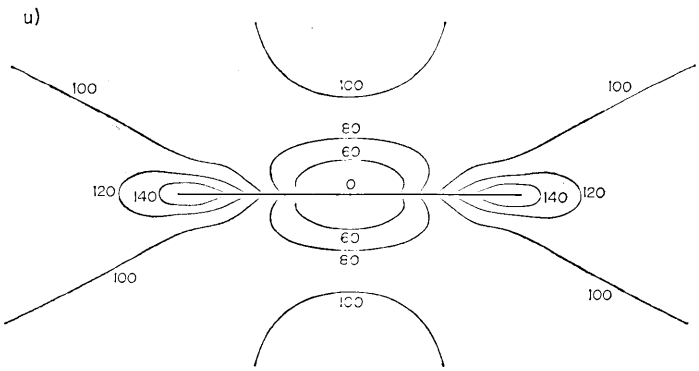

Fig. 14. u) Contours of equal maximum shear stress.

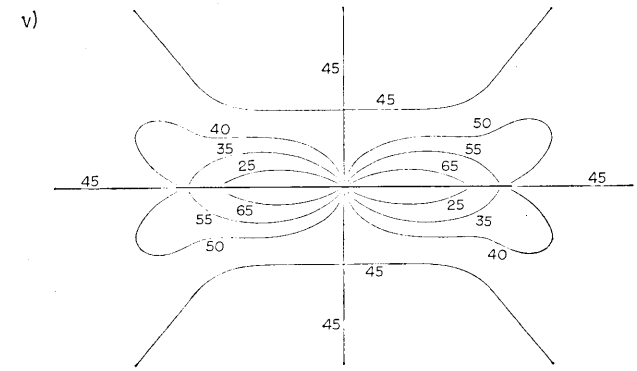

Fig. 14. v) Contours of equal direction of maximum tension. Contour values are in units of degrees, measured counterclockwise from the direction of x-axis.

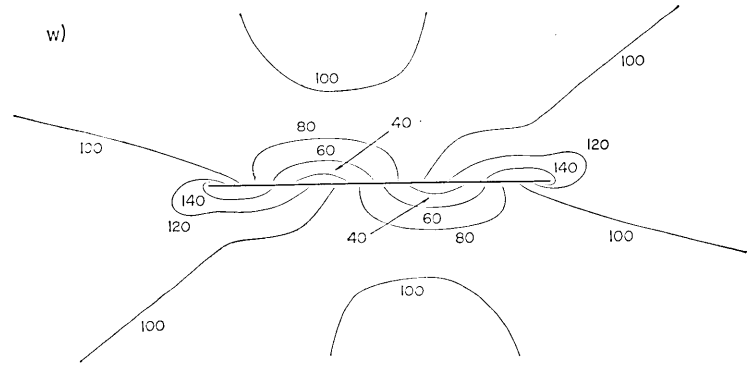

Fig. 15. w) Contours of equal maximum shear stress.

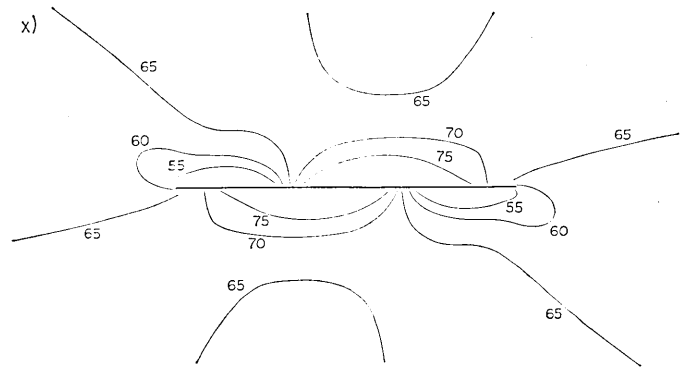

Fig. 15. x) Contours of equal direction of maximum tension. Contour values are in units of degrees, measured counterclockwise from the direction of x-axis.

6. Concluding remarks

(1) The most remarkable feature seen from the preceding maps is that the stress field around a crack is fairly complicated. There are always regions where certain components of stress are not decreased but increased by the introduction of a crack. This may be one of the conclusions which are valid to some extent even if non-elastic properties of the substance are taken into consideration. This is very interesting in view of the fact that an ordinary shallow earthquake is usually accompanied by aftershocks.

(2) Some of the relations between the functional form of tangential discontinuity in displacement on a crack and the corresponding stress distribution are clearly demonstrated in the maps obtained. In the neighborhood of the right end of the crack we can see that

$$\begin{aligned} &(\mathrm{i}) \quad \Delta u \propto |a-\xi|^{0} \quad \text{in} \quad (3.1), \\ &(\mathrm{ii}) \quad \Delta u \propto |a-\xi|^{1/2} \quad \text{in} \quad (4.1), \\ &(\mathrm{iii}) \quad \Delta u \propto |a-\xi|^{3/2} \quad \text{in} \quad (5.6). \end{aligned}$$

We have called the forms in (3.1) and (4.1) rectangular and elliptic type respectively. One of the characteristic differences between the stress distributions due to these three dislocations can be found in maps of maximum shear stress. If we compare the shapes of contours around the ends between Fig. 6, (1); Fig. 8, d); and Fig. 14, u), changes by degrees in accord with the exponents of $|a-\xi|$ are seen: shape of two circles in contact, shape of a section of a gourd, and shape of a section of an acorn. This change can be said to be in the direction to level high mountains and deep valleys of the stress distribution.

(3) Though we treated two-dimensional problem, the principal features around a slip type crack are similar to those at the free surface around a strike slip faulting in a semi-infinite elastic solid. It is interesting to compare our Figures with those by Chinnery: Fig. 8, c) with Fig. 2 of Chinnery (1963), and Figs. 8, d); 12, s); 8, f); 12, t) with Figs. 4a, 4b, 5a, 5b of Chinnery (1966) respectively. If we compare Figs. 8, d) and 14, u) with Figs. 7b and 7c of Chinnery and Petrak (1968), we can see that the main differences in the features around the crack end come from the differences in the type of discontinuity in displacement. Except the last example, the discontinuity in ours is of elliptic type, while in Chinnery's of rectangular type.

(4) The fundamental features of the stress field at the end of a crack caused by a displacement discontinuity of elliptic type are seen to some extent from those due to a displacement discontinuity of rectangular type. For example, applying equations (3.7) to the cases, we have

$$\chi=0°,\quad 30°,\quad -45°,\quad -30°,$$

in the cases of Fig. 8, 9, 10, 11 respectively. If we compare the above values of χ with the direction of gourd-shaped contours in the neighbourhood of the end of the crack in Fig. 8, d); 9, j); 10, m); 11, p), the similarity is obvious.

(5) If we apply equations (3.7) to the case of Fig. 15, we have $\chi=0$. But on the Fig. 15, w), we can not expect at the ends gourd-shaped contours placed in the direction of the x-axis. It seems that the stress field in the direct neighborhood of the end in this case is fairly different from the case of rectangular discontinuity. This is a case where the stresses have finite values at the ends. At a distance, the stress distribution is much similar to that of elliptic or rectangular discontinuity.

(6) We can conclude that the usefulness of the two-dimensional theory of elastic dislocations is demonstrated for a single crack introduced in a purely elastic homogeneous medium. In actual cases as we meet with in the Earth's interior or in rocks, many cracks will exist in a body of non-elastic property, but a knowledge concerning idealized problems treated in the present study will play some rôle in those cases.

7. Appendix

7.1 Comparison of equations (4.6) with Starr's formulas

Starr's (1928) formulas are referred to elliptic coordinates ξ, η which are defined by

$$z=c\cosh\zeta,\qquad z=x+iy,\qquad \zeta=\xi+i\eta, \tag{7.1}$$

or

$$x=c\cosh\xi\cos\eta,\qquad y=c\sinh\xi\sin\eta. \tag{7.2}$$

For a constant value of ξ we obtain an ellipse of semiaxes $c\cosh\xi$, $c\sinh\xi$ with foci at $x=\pm c$, while for a constant value of η a hyperbola with the same foci. From (7.2) we have

$$\begin{cases} \dfrac{\partial x}{\partial\xi}=c\sinh\xi\cos\eta & \dfrac{\partial y}{\partial\xi}=c\cosh\xi\sin\eta \\ \dfrac{\partial x}{\partial\eta}=-c\cosh\xi\sin\eta & \dfrac{\partial y}{\partial\eta}=c\cosh\xi\cos\eta. \end{cases} \tag{7.3}$$

The modulus of transformation h is then given by

$$\frac{1}{h^2}=\left(\frac{\partial x}{\partial \xi}\right)^2+\left(\frac{\partial x}{\partial \eta}\right)^2=\frac{\partial(x,\,y)}{\partial(\xi,\,\eta)}=c^2(\cosh^2\xi-\cos^2\eta). \tag{7.4}$$

Coordinates r_1, r_2, θ_1, θ_2 (Fig. 16) and elliptic coordinates are related as

$$r_1=c(\cosh\xi-\cos\eta), \qquad r_2=c(\cosh\xi+\cos\eta), \tag{7.5}$$

$$\cos\left(\frac{\theta_1+\theta_2}{2}\right)=ch\,\sinh\xi\cos\eta, \qquad \sin\left(\frac{\theta_1+\theta_2}{2}\right)=ch\,\cosh\xi\sin\eta. \tag{7.6}$$

The last equations (7.6) may be obtained, if we compare (7.3) with the following scheme of direction cosines of the tangents to the curves η =constant and ξ=constant, which are taken in the directions ξ-increasing and η-increasing respectively (Fig. 16).

	x	y
ξ	$\cos\left(\frac{\theta_1+\theta_2}{2}\right)$	$\sin\left(\frac{\theta_1+\theta_2}{2}\right)$
η	$-\sin\left(\frac{\theta_1+\theta_2}{2}\right)$	$\cos\left(\frac{\theta_1+\theta_2}{2}\right)$

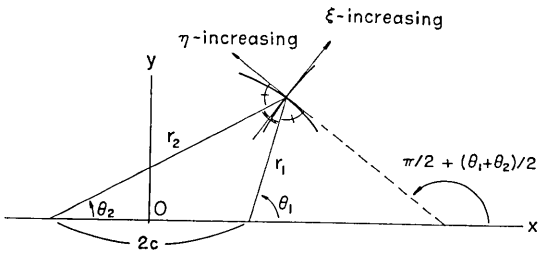

Fig. 16. Coordinates r_1, r_2, θ_1, θ_2 and directions of tangents to the ellipse and the hyperbola which determine the elliptic coordinates ξ, η.

From (7.4) and (7.5) we have

$$h=\frac{1}{\sqrt{r_1 r_2}}. \tag{7.7}$$

When the elliptic crack in Starr's paper (1928) becomes a line of length 2c connecting the foci, i.e. $\xi_0=0$ in equation (13)*, the displacement vector with respect to elliptic coordinates is

* The factor $(\cos 2\eta-e^{-\xi})$ in the last term of the second equation of (13) in Starr's paper (1928) should be read $(\cos 2\eta-e^{-2\xi})$.

$$\begin{cases} u_\xi = \dfrac{1}{4}\dfrac{1}{\mu} Sc^2 h \sinh 2\xi \sin 2\eta + \dfrac{1}{4}\dfrac{\lambda+2\mu}{\mu(\lambda+\mu)} Sc^2 h \sin 2\eta \\ u_\eta = \dfrac{1}{4}\dfrac{1}{\mu} Sc^2 h (\cosh 2\xi - 1)\cos 2\eta + \dfrac{1}{4}\dfrac{\lambda+2\mu}{\mu(\lambda+\mu)} Sc^2 h (\cos 2\eta - e^{-2\xi}). \end{cases} \tag{7.8}$$

If these components are transformed to the x- and y- components by use of the foregoing relations,

$$\begin{cases} 2\mu u = S\left[\dfrac{\kappa+1}{2}\left(\sqrt{r_1 r_2}\sin\dfrac{\theta_1+\theta_2}{2} - y\right)\right. \\ \qquad\qquad \left. + y\left\{\dfrac{r}{\sqrt{r_1 r_2}}\cos\left(\theta - \dfrac{\theta_1+\theta_2}{2}\right) - 1\right\} + y\right] \\ 2\mu v = S\left[-\dfrac{\kappa-1}{2}\left(\sqrt{r_1 r_2}\cos\dfrac{\theta_1+\theta_2}{2} - x\right)\right. \\ \qquad\qquad \left. - y\left\{\dfrac{r}{\sqrt{r_1 r_2}}\sin\left(\theta - \dfrac{\theta_1+\theta_2}{2}\right)\right\} + x\right]. \end{cases} \tag{7.9}$$

This displacement field is exactly the same as equations (4.6) but an additive field

$$\begin{cases} 2\mu u = Sy \\ 2\mu v = Sx, \end{cases} \tag{7.10}$$

if we replace c by a and take

$$S = \frac{2\mu}{\kappa+1}\frac{U}{a}. \tag{7.11}$$

u and v given by (7.10) are nothing but the displacement added to equations (4.6) in order to make the stress free on the prescribed crack.

7.2 Comparison of the Fig. 10, m) with a photograph after Duda

Figure 17 is a copy printed from the reverse side of the negative taken from a photograph in Duda's paper (1965), which is originally given in color. In this photoelastic experiment by S. J. Duda, transparent plates, with a slit located in the center of the plate and oriented along a diagonal, were put under stress. The plate shown in Fig. 17 has the dimension of 18 cm×18 cm×1cm (thickness) and the slit of 3.8 cm×0.1 cm (width)×0.8 cm (depth). This slit is a closed one, consisting of cuts from either side, 0.4 cm deep. Duda considered that the closed slit corresponds to a zone of weakness. We can imagine from Fig. 17 that the isochromatics in the original photograph have a shape very much resembling the contour lines in Fig. 10, m), in which the contour lines

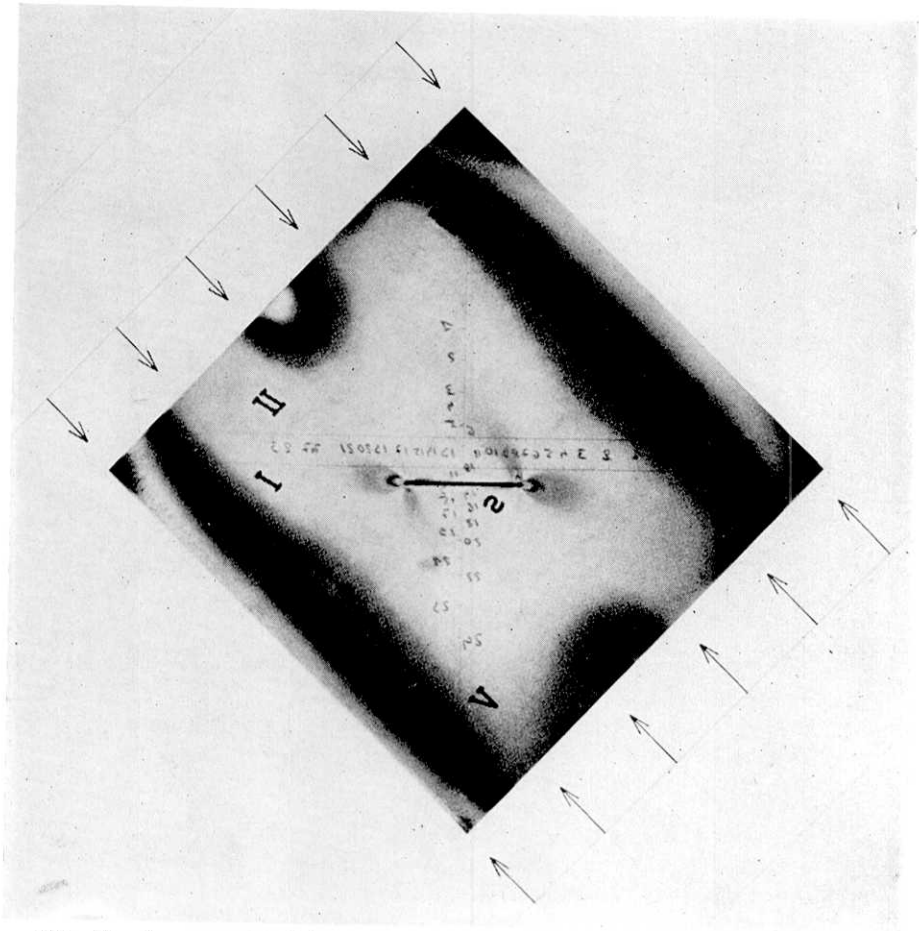

Fig. 17. A copy printed from the reverse side of the negative taken from a color photograph in Duda's paper (1965).

are of equal maximum shear stress around an open crack in a uniaxial applied pressure. Strictly speaking, the plate in the experiment is neither in the state of plane strain nor in that of the generalized plane stress. Since, however, the state of stress is approximately two-dimensional, the resemblance of the photograph to the result of calculation must be very good. For a detailed comparison reference to the original photograph is desirable.

8. Acknowledgments

The author wishes to express his sincere thanks to professor Yasuo Satô who encouraged the author to complete the work, read the manu-

script and suggested several improvements. Thanks are also due to Dr. Kiyoo Mogi who called the author's attention to the maps of maximum tension and Dr. Seweryn J. Duda and Editors of the Geophysical Journal of the Royal Astronomical Society who permitted the reproduction of the original photograph.

9. References

AKI, K., 1966, Generation and propagation of G waves from the Niigata earthquake of June 16, 1964, Part 2, Estimation of earthquake moment, released energy, and stress-strain drop from the *G* wave spectrum, *Bull. Earthq. Res. Inst.*, **44**, 73-88.

ANDERSON, E. M., 1951, *Dynamics of Faulting*, 2nd ed., Oliver and Boyd, London.

BARENBLATT, G. I., 1962, The mathematical theory of equilibrium cracks in brittle fracture, in *Advances in Applied Mechanics*, **7**, 55-129, Academic Press, New York.

CHINNERY, M. A., 1961, The deformation of the ground around surface faults, *Bull. Seism. Soc. Amer.*, **51**, 355-372.

CHINNERY, M. A., 1963, The stress changes that accompany strike-slip faulting, *Bull. Seism. Soc. Amer.*, **53**, 921-932.

CHINNERY, M. A., 1966, Secondary faulting, 1, Theoretical aspects, *Can. J. Earth Sci.*, **3**, 163-174.

CEINNERY, M. A., and J. A. PETRAK, 1968, The dislocation fault model with a variable discontinuity, *Tectonophysics*, **5**, 513-529.

DUDA, S. J., 1965, The stress around a fault according to a photoelastic model experiment, *Geophys. J.*, **9**, 399-410.

ESHELBY, J. D., 1956, The continuum theory of lattice defects, in *Solid State Phys.*, **3**, 79-144, Academic Press Inc.

GREEN, A. E., and W. ZERNA, 1954, *Theoretical Elasticity*, Oxford Univ. Press.

INGLIS, C. E., 1913, Stresses in a plate due to the presence of cracks and sharp corners, *Trans. Inst. Naval Arch.*, **55**, Part 1, 219-230.

KASAHARA, K., 1957, The nature of seismic origins as inferred from seismological and geodetic observations (1), *Bull. Earthq. Res. Inst.*, **35**, 473-532.

KNOPOFF, L., 1958, Energy release in earthquakes, *Geophys. J.*, **1**, 44-52.

MARUYAMA, T., 1963, On the force equivalents of dynamical elastic dislocations with reference to the earthquake mechanism, *Bull. Earthq. Res. Inst.*, **41**, 467-486.

MARUYAMA, T., 1964, Statical elastic dislocations in an infinite and semi-infinite medium, *Bull. Earthq. Res. Inst.*, **42**, 289-368.

MARUYAMA, T., 1966, On two-dimensional elastic dislocations in an infinite and semi-infinite medium, *Bull. Earthq. Res. Inst.*, **44**, 811-871.

MUSKHELISHVILI, N. I., 1953, *Some Basic Problems of the Mathematical Theory of Elasticity*, (translated from the Russian), P. Noordhoff, Groningen, Holland.

PRESS, F., 1965, Displacements, strains, and tilts at teleseismic distances, *J. Geophys. Res.*, **70**, 2395-2412.

SAVIN, G. N., 1961, *Stress Concentration around Holes*, (translated from the Russian), Pergamon Press, New York.

SNEDDON, I. N., 1964, The distribution stress in the neighbourhood of a crack in an elastic solid, *Proc. Roy. Soc. London, Ser. A*, **187**, 229-260.

SENDDON, I. N., 1951, *Fourier Transforms*, McGraw-Hill Book Co., Inc., New York.

STARR, A. T., 1928, Slip in a crystal and rupture in a solid due to shear, *Proc. Cambridge Phil. Soc.*, **24**, 498-500.

STEKETEE, J. A., 1958a, On Volterra's dislocation in a semi-infinite elastic medium, *Can. J. Phys.*, **36**, 192-205.

STEKETEE, J. A., 1958b, Some geophysical applications of the theory of dislocations, *Can. J. Phys.*, **36**, 1168-1198.

VVEDENSKAYA, A. V., 1956, The determination of the displacement field of earthquakes by use of dislocation theory (in Russian), *Izv. Akad. Nauk SSSR, Ser. Geofiz.*, 277-284.

---

1. 割れ目付近の応力場

地震研究所　丸　山　卓　男

等方均質な弾性体の中に割れ目を導入したときの割れ目付近の応力場を，2次元の問題として扱った．平面ひずみまたは平面応力の仮定をとる．この仮定は，基本方程式を分類したときの筆者の前論文 (1966) の呼び名では System II に当る．Kasahara, Knopoff が扱ったような変位が紙面に垂直である2次元の割れ目の場合には触れていない．これは先の呼び名に従えば System I の場合で，その応力場は本論の場合よりも簡単である．また本論は，線型理論の範囲にとどまり，割れ目の先端が応力場の作用で成長する場合の非線型問題には立ち入らない．

割れ目を2次元の Somigliana のくいちがいと一様な応力場との重ね合わせとして表現し，割れ目の上の境界条件によって分類したとき，この面が自由表面である場合と，接している面が相互にすべるだけで，離れたりくいこんだりはしない場合の2つのモデルを主に扱った．応力場の計算には，筆者の前論文 (1966) で得た式を利用し，結果をいくつかの図に示した．割れ目と最大圧力の方向のなす角は 45° か 30° (または 25°) である．本論の主要な目的はこれらの図を提供することにある．

さしあたり，これらの図から導かれる結論を列挙すれば次の通りである．

(1) 割れ目付近の応力場はかなり複雑であって，割れ目を導入することによって，応力のある成分が増大するような部分がある．この特性は物質の非弾性的性質を考慮してもある程度なり立つことにちがいない．このことは，浅い地震が一般に余震をともなうことに対応して非常に興味深い．

(2) 本論で扱った，割れ目の上での変位の不連続 (くいちがい) のいくつかの関数形に対応して，応力場にあらわれる相違が注目される．接線方向へのくいちがい Δu について見て，割れ目の端 ($x=a$) の付近で $\Delta u \propto |x-a|^{\alpha}$ とするとき，$\alpha=0,\ 1/2,\ 3/2$ に対応して，最大接線応力の分布を示すコントルに，相接する2円，ひょうたん型，どんぐり型が現われている．この変化は応力場の山谷をならす向きに当たる．

(3) 半無限弾性体の横すべり型断層模型の場合の地表付近の応力場に関する Chinnery らの計算と比較すると，顕著な類似が指摘できる．このことは2次元化による簡単化の有用性を示すものでもある．

(4) 割れ目の面の上での一定の接線応力，法線応力に対応するくいちがい，すなわち Δu や Δv が $(a^2-\xi^2)^{1/2}$ の関数形 (割れ目の長さを $2a$，割れ目の中心からの距離を ξ として) を持つ場合，割れ目の端点での応力場は，Δu, Δv を階段的変化とした場合の簡単な応力場から推定できる．本論で述べた方法は簡単であるから有用性が期待できる．

(5) 端点で応力が無限大にならない1つの場合，$\Delta u \propto (a^2-\xi^2)^{3/2}$ のときには，端点付近の応力場は (4) とは少し異なったものとなる．この場合は先の応力場の山谷をある程度ならすことによって推定できよう．遠方に行くと，Δu の関数形による相違は小さくなる．

(6) このようにして，割れ目の模型の問題を，2次元の Somigliana のくいちがいと一様な応力場との重ね合わせによって表わす方法は，種々の割れ目の付近の応力場を統一的に理解する上で有効なものであるといってよい．

最後の部分に，本論の中に用いた1つの式と Starr による式との一致，Duda が光弾性実験で得た isochromatics と本論の中の1つの計算結果との一致について，付記を加えた．